Clay Minerals (2023), **58**, 364–377
doi:10.1180/clm.2023.33

CAMBRIDGE UNIVERSITY PRESS

Article

Characterization of the clayey sediments in the exposed mudflats of the western Dead Sea shore

Shlomo Shoval[1,2]

[1]Earth Sciences, Geology Group, Department of Natural Sciences, The Open University of Israel, Raanana, Israel and [2]Visiting Scientist, Freddy and Nadine Herrmann Institute of Earth Sciences, The Hebrew University of Jerusalem, Jerusalem, Israel

Abstract

The retreat of the Dead Sea and the lowering of the base level in recent decades have led to the exposure of the littoral clay sediments on the shore, the occurrence of exposed mudflats and the development of ground subsidence along strips ('subsidence strips') and clustered sinkholes. Based on field observations and laboratory analyses, the present study characterizes the clayey sediments in the environment of the exposed mudflats on the western Dead Sea shore. The clayey sediments of the exposed mudflats ('mudflat sediments') consist of fine-grained laminated calcareous clays. The mineral composition of the bulk mudflat sediments consists of clay and carbonate minerals (calcite, aragonite and dolomite) with some quartz and feldspar, and frequently gypsum and halite. The clay mineral composition of these samples is smectitic illite–smectite and kaolinite with some discrete illite and palygorskite. The smectitic illite–smectite is randomly interstratified (1.7 nm illite–smectite type R = 0). Although the detrital smectitic illite–smectite in the mudflat sediments is situated in the saline environment of the Dead Sea shore, no significant illitization is observed in the depositional detrital clay. Subsidence strips with clustered sinkholes were formed in the exposed mudflats as part of the adjustment of the Dead Sea periphery to the lowering of the base level as a result of the retreat. The field observations in the studied area reveal that the subsiding of mudflat sediments in the formation of the subsidence strips usually involves mud sagging of wet clayey sediments in the subsurface and sediment collapse of dry clayey sediments near the surface.

Keywords: Clay analysis; clustered sinkhole; littoral sediment; mud sagging; mudflat sediment; saline environment; sediment collapse; subsidence strip

(Received 12 May 2023; revised 13 November 2023; Accepted Manuscript online: 24 November 2023; Associate Editor: Asuman Türkmenoğlu)

The Dead Sea is a hypersaline terminal desert lake located in the Dead Sea Valley and terminates the drainage system of the Jordan River (Fig. 1). The Dead Sea Valley is the lowest exposed land on Earth. From a geological point of view, the Dead Sea Basin is an active pull-apart basin located within the morphotectonic depression of the Dead Sea Rift (Garfunkel & Ben-Avraham, 1996; Garfunkel, 1997). The Dead Sea includes the northern deep Dead Sea (Fig. 1b), with the deepest submarine bottom point today at ~730 m below the mean sea or ocean level (BMSL) and the southern shallow part separated by the Lisan Peninsula and occupied by evaporation ponds (Neev & Hall, 1979).

A generalized geological map of the Dead Sea Basin and adjacent regions is presented in Fig. 2. The main units exposed at the margins of the Dead Sea Basin are Upper Cretaceous carbonate rocks (Fig. 2). On the eastern side of the Dead Sea Basin, Cambrian to Lower Cretaceous clastic rocks are also exposed.

The main units exposed in the periphery of the Dead Sea are Late Neogene–Quaternary (Fig. 2). These units are classified in the Dead Sea Group, which comprises clastic, detrital, evaporitic, lacustrine and fluvial sediments (Stein, 2001). This group includes the Sedom, Amora, Samra, Lisan and Ze'elim formations, which were deposited from the Late Neogene Sedom Lagoon (Shoval & Zlatkin, 2009), throughout the Quaternary lakes of Amora, Samra and Lisan and up to the Holocene Dead Sea (Bookman *et al.*, 2004; Stein, 2014).

The Holocene clayey sediments of the mudflats studied here are classified in the stratigraphic unit 'Ze'elim Formation' (Yechieli *et al.*, 1993; Stein, 2014). This Formation also consists of gravel deposits that occur in alluvial fans. The Ze'elim Formation reaches a thickness of ~20–30 m in the north-western Dead Sea shore and ~80 m in the south-western part (Stein, 2001). A subsurface salt-rock unit, ~20–30 m thick, usually occurs at the base of the Ze'elim Formation (Yechieli *et al.*, 2003, 2006; Abelson *et al.*, 2006; Stein, 2014; Avni *et al.*, 2016).

The clayey sediments of the Ze'elim Formation are characterized by a fine-grained laminated texture, in which a dark lamina of detritus alternates with a light lamina of authigenic minerals (Bookman *et al.*, 2004). The laminated texture reflects seasonal deposition (Lu *et al.*, 2020). The dark lamina consists of transported detritus material: clay minerals and fine-grained calcite and dolomite (Garber *et al.*, 1987; Bookman *et al.*, 2004). The light lamina consists of precipitated authigenic aragonite and frequently gypsum and halite

Email: shovals@openu.ac.il
Cite this article: Shoval S (2023). Characterization of the clayey sediments in the exposed mudflats of the western Dead Sea shore. *Clay Minerals* **58**, 364–377. https://doi.org/10.1180/clm.2023.33

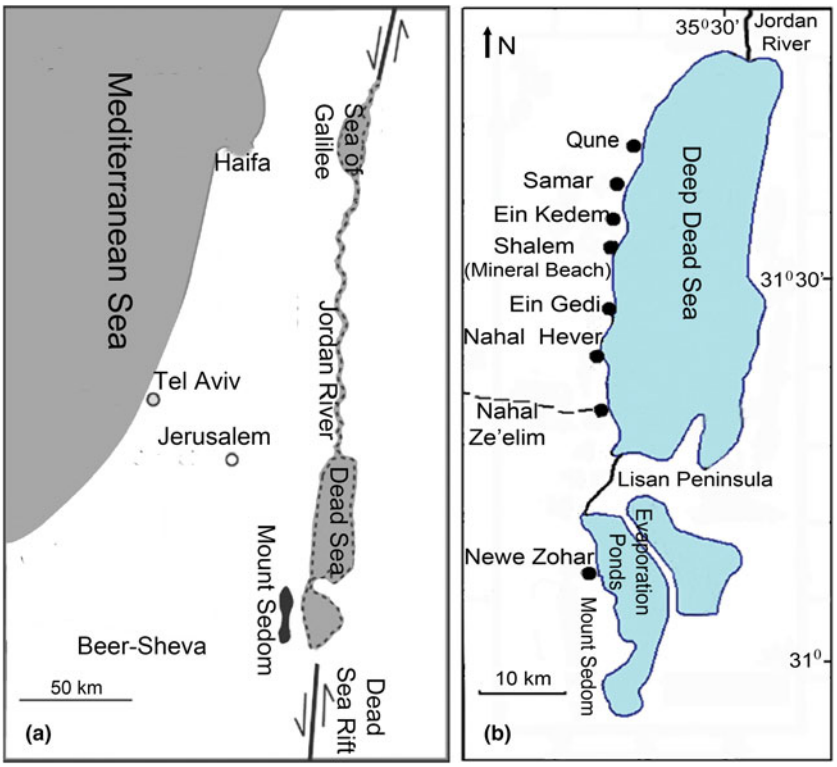

Figure 1. The Dead Sea region. (a) Location map of the Dead Sea. (b) Site map of the Dead Sea area.

(Belmaker *et al.*, 2019). Reports on the clays of the Dead Sea were made by Nathan *et al.* (1990, 1992, 1994). Clays of the north-eastern shores of the Dead Sea were analysed by Salameh *et al.* (2019).

In recent decades, the Dead Sea has been subject to a rapid drop in water level (e.g. Lipchin *et al.*, 2004; Vey *et al.*, 2021) and rapid retreat (Arkin & Gilat, 2000; Ghazleh *et al.*, 2011).

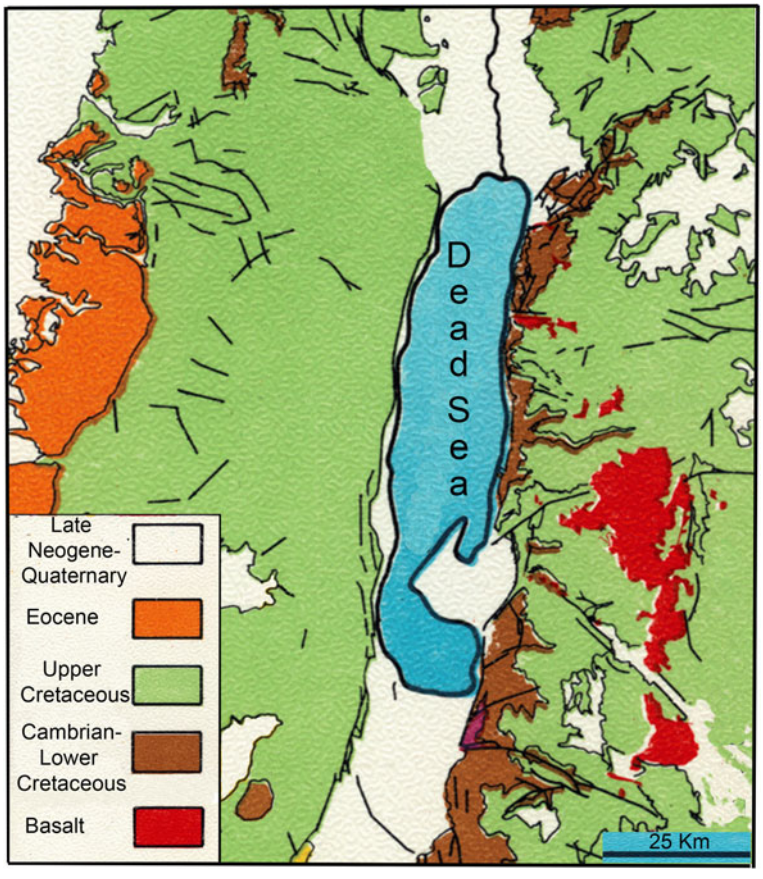

Figure 2. Generalized geological map of the Dead Sea Basin and adjacent regions (modified from the generalized geological map of Israel of the Geological Survey of Israel).

During the last 47 years, the water level of the Dead Sea has dropped by ~39 m and on 1 September 2023 was −438.21 m BMSL (https://data.gov.il/dataset/https-www-data-gov-il-dataset-683/resource/823479b4-4771-43d8-9189-6a2a1dcaaf10). These processes led to the exposure of the littoral clayey sediments on the shore, the occurrence of exposed mudflats (e.g. Arkin & Gilat, 2000), the development of subsidence features (Baer *et al.*, 2002; Yechieli *et al.*, 2003, 2006, 2016; Abelson *et al.*, 2006; Al-Halbouni *et al.*, 2017; Shviro *et al.*, 2017; Vey *et al.*, 2021) and the emergence of sinkholes (e.g. Abelson, 2021; Ezersky & Frumkin, 2021).

Most of this previous work relates to the origins of the Dead Sea sinkholes. The present study characterizes the clayey sediments in the environment of the exposed mudflats on the western Dead Sea shore based on field observations and laboratory analyses. The mineral composition and the clay mineral composition of the mudflat sediments sampled from subsidence strips and in clustered sinkholes are analysed, the effect of the saline environment on the clay minerals is examined and the contribution of the clayey sediments to the origins of the subsidence strips is investigated.

Field observations

Clayey sediments of the exposed mudflats

Exposed mudflats have been occurring in recent decades on the western shore of the Dead Sea as part of the adjustment of the Dead Sea periphery to the retreat of the Dead Sea. Figure 3 demonstrates clayey sediments of the exposed mudflats on the Dead Sea shore in the studied area. The mudflat sediments were deposited in a lacustrine–littoral environment of the Dead Sea periphery (Yechieli *et al.*, 1993). They were exposed on the shore in recent decades as a result of the retreat of the Dead Sea (Fig. 3a). Exposed mudflats with lines of coastal regression herald the progressive retreat of the Dead Sea (Fig. 3a). A fine-grained laminated texture of the mudflat sediments is observed on the walls of the sinkholes.

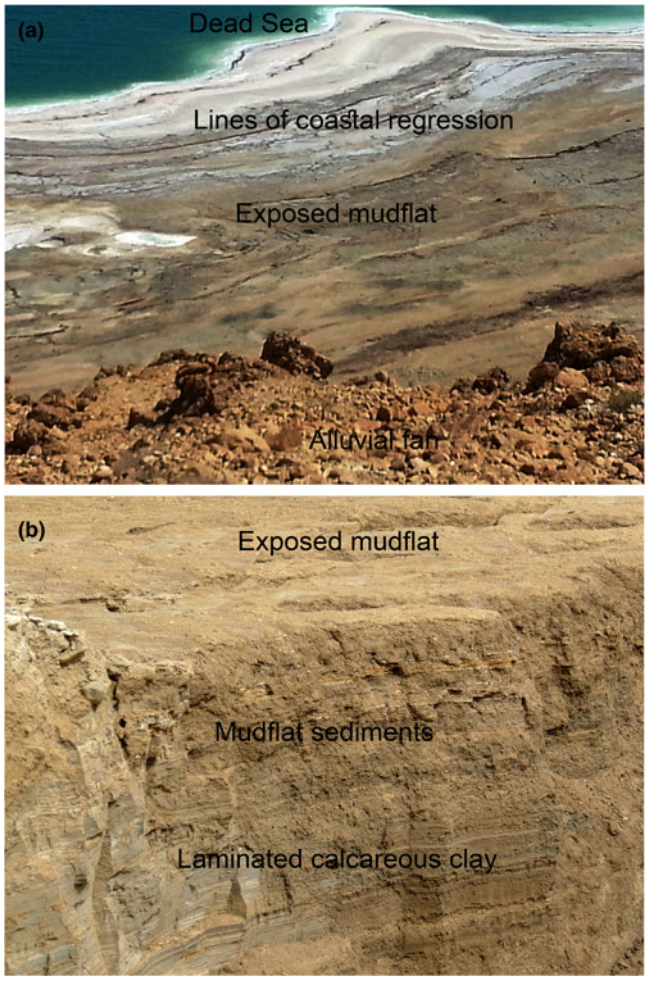

Figure 3. Clayey sediments of the exposed mudflats on the Dead Sea shore in the studied area. (a) Exposed mudflats with lines of coastal regression herald the progressive retreat of the Dead Sea (north of Ein Gedi coast). (b) A fine-grained laminated texture of the mudflat sediments is observed on the walls of the sinkholes (at Shalem coast).

Subsidence strips with sinkholes in the exposed mudflats

Figure 4 demonstrates subsidence strips with clustered sinkholes in the exposed mudflats in the studied area. These features extend approximately parallel to the shoreline; they gradually widen over time and progressively inundate with saline water. The sinkholes evolved from narrower holes with steep walls to widening ones and to coalesced sinkholes (Fig. 4a). A collapse in the mudflat sediments is observed on the walls of the sinkholes (Fig. 4b).

The saline environment of the mudflat sediments

The saline environment of the mudflat sediments in the studied area is indicated by accumulation of brine and precipitation of salts at the bottoms of subsidence strips and in sinkholes (Fig. 5). The mineral precipitates from the sinkhole brine are halite and gypsum, with some carnallite and bischofite (Zilberman-Kron, 2008).

Experimental

Materials

Table 1 presents the list of the analysed mudflat sediments sampled from subsidence strips and in clustered sinkholes (Fig. 4). Samples of sinkhole brine (Fig. 5), local saline water and sea water were also collected (Table 1). The sampling sites are Ein Samar, Shalem and Ein Gedi coasts (Fig. 1b).

For the analysis of the mineral composition, the samples of the mudflat sediments were homogenized using a ball shaker. For the analysis of the clay mineral composition, decalcified clay fractions from the samples of the mudflat sediments were obtained according to the standard preparation protocol (Eslinger & Pevear, 1988; Moore & Reynolds, 1997).

Methods

The clayey sediments in the environment of exposed mudflats on the western Dead Sea shore were analysed using mineralogical and chemical methods. Mineralogical and chemical methods for the study of clayey rocks and clayey sediments have recently been applied by Trindade *et al.* (2013, 2018), Leontopoulou *et al.* (2021) and Rogoziński & Maciejewska (2021).

Details of the analysing methods in our experiments are described by Shoval & Zlatkin (2009). The samples were analysed using X-ray powder diffraction (XRD) with a Philips PW-3710 diffractometer using Cu-*K*α radiation at 35 kV and 40 mA and

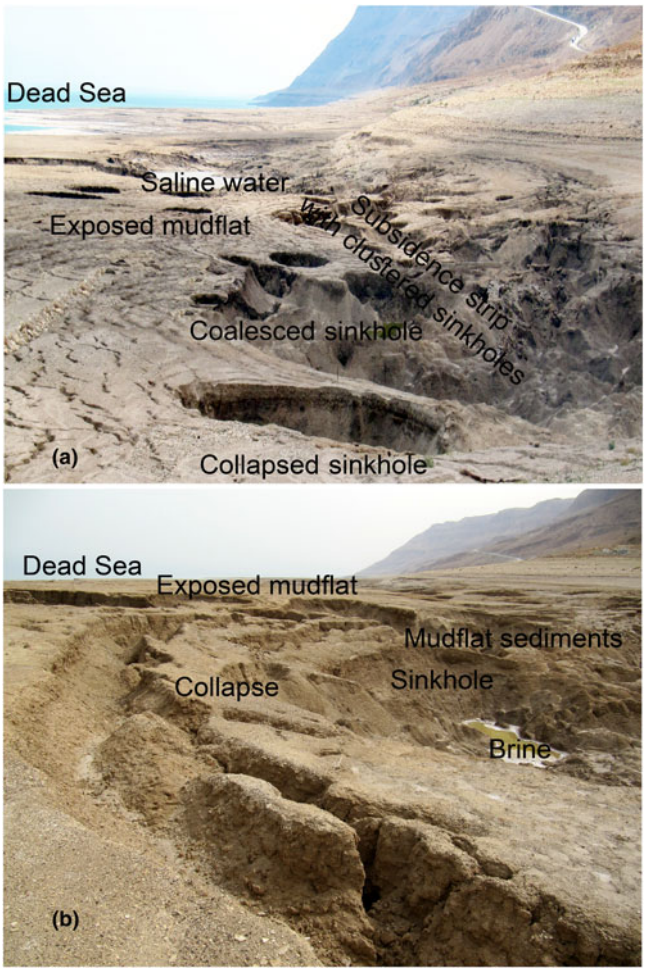

Figure 4. Subsidence strips with clustered sinkholes in the exposed mudflats in the studied area. (a) The sinkholes evolved from narrower holes with steep walls to widening ones and to coalesced sinkholes (at Shalem coast). (b) A collapse in the mudflat sediments is observed on the walls of the sinkholes (at Shalem coast).

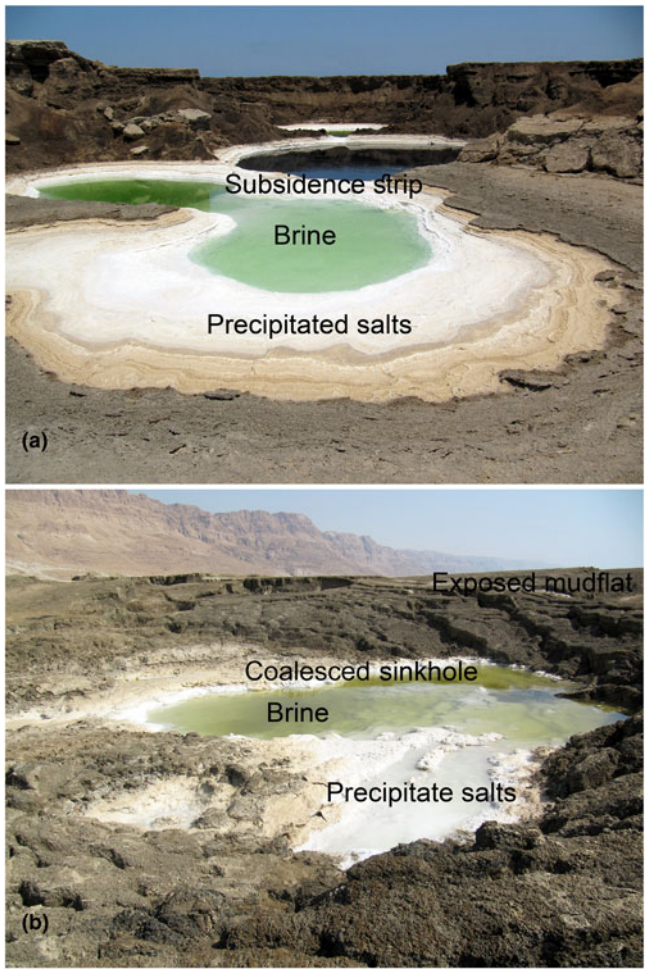

Figure 5. The saline environment of the mudflat sediments in the studied area is indicated by accumulation of brine and precipitation of salts at the bottom of (a) subsidence strips (at Ein Gedi coast) and (b) in sinkholes (at Shalem coast).

a curved graphite monochromator. Fourier-transform infrared (FTIR) spectroscopy was conducted using a Jasco-4100 FTIR spectrometer with pressed KBr discs of 1 mg of the powdered sample and 150 mg of KBr. Scanning electron microscopy (SEM) was conducted using a JEOL SEM (JSM-840) microscope equipped with a LINK-10000 energy-dispersive spectrometer (EDS; Oxford ISIS), using carbon-coated samples. The saline water types were analysed using wet chemical analysis methods. The concentrations of Na, K, Ca, Mg and Sr were obtained using a Perkin Elmer inductively coupled plasma–optical emission spectrometer (Optima 3300); that of Br was obtained using a Dionex (4000I) ion chromatograph; and that of Cl was obtained *via* titration with a Metrohm (Titroprocessor 636) apparatus.

Curve-fitting of the XRD traces and the FTIR spectra was performed using the *GRAMS/AI 32* software package of Thermo Electron Corporation (Shoval *et al.*, 1999; Shoval & Zlatkin, 2009).

Results

XRD analysis of the bulk mudflat sediments

Figure 6 demonstrates XRD traces of selected mudflat sediments sampled from subsidence strips and clustered sinkholes. The bulk mudflat sediments consist of clay minerals and carbonates (calcite, aragonite and dolomite) with some quartz and feldspar, and frequently gypsum and halite (Fig. 6).

Table 2 presents the XRD results of the relative amounts of the minerals present in the bulk mudflat sediments sampled from subsidence strips and in clustered sinkholes. The determination of the relative amounts of these minerals in the bulk mudflat sediments is based on the peak height (counts s^{-1}) of the major XRD peak of each mineral (Fig. 6) using the apparatus's software. Table 2 includes the *d* (nm)/°2θ values of the major XRD peak for each of the identified minerals and the conversion factors used to calculate the proportions of the various minerals (Ganor *et al.*, 2000). The factors used were determined under conditions used in the operating Geological Survey of Israel laboratory and based on calibrations with known proportions of local minerals (thus, the conversion factors are not universally applicable between laboratories).

FTIR spectroscopy analysis of the bulk mudflat sediments

Figure 7 shows the FTIR spectra in the range 1800–400 cm^{-1} of selected mudflat sediments. The FTIR spectroscopy results confirm the presence of clay minerals, calcite, aragonite, quartz and frequently gypsum in these sediments (Fig. 7). The minerals

Table 1. List of the analysed mudflat sediments sampled from subsidence strips and in clustered sinkholes. Samples of sinkhole brine, local saline water and sea water were also collected.

Mudflat sediments In subsidence strips (S-)	Locations	Saline water Sinkhole brine (B-)	Locations
S-ES-1, S-ES-2, S-ES-3	Ein Samar coast (ES-)	B-ES-1	Ein Samar coast
S-EG-1, S-EG-2	Ein Gedi coast (EG-)	B-MB-14, B-MB-15, B-MB-16	Shalem coast
S-MB-1, S-MB-2, S-MB-3, S-MB-4, S-MB-5	Shalem coast (MB-)	B-EG-7, B-EG-8, B-EG-9	Ein Gedi coast
In clustered sinkholes (H-)		*Local saline water (W-)*	
H-ES-4, H-ES-5, H-ES-6, M-ES-7	Ein Samar coast	W-ES-2, W-ES-3	Ein Samar coast
H-EG-3, H-EG-4, H-EG-5, M-MB-7	Ein Gedi coast	W-EG-4	Ein Gedi coast
H-MB-8, H-MB-12	Shalem coast	*Sea water*	
		W-DS-1	Dead Sea water (DS-)
		W-MS-1	Mediterranean Sea water (MS-)

were identified by their characteristic bands in the FTIR spectra, supported by spectral standards of minerals (Farmer, 1974; Shoval, 2017).

Clay mineral composition in decalcified clay fractions

The clay mineral composition in decalcified clay fractions obtained from the mudflat sediments was analysed using XRD and FTIR spectroscopy. The clay mineralogy was determined on air-dried, ethylene glycol-solvated oriented clay fractions before and after heating at 550°C for 2 h (Eslinger & Pevear, 1988). Figure 8 shows XRD traces of the clay fraction obtained from a selected mudflat sediment before and after baseline correction and curve-fitting with *GRAMS/AI 32* software (Fig. 8a & 8b, respectively). The clay minerals identified are smectite-rich R0 mixed-layer illite–smectite and kaolinite with some discrete illite and palygorskite (Fig. 8). The identification of R0 mixed-layer illite–smectite is based on the (001) diffraction maxima at ~1.7 nm after ethylene glycol solvation (Table 3) and on the asymmetry and the width of this peak in the original XRD traces

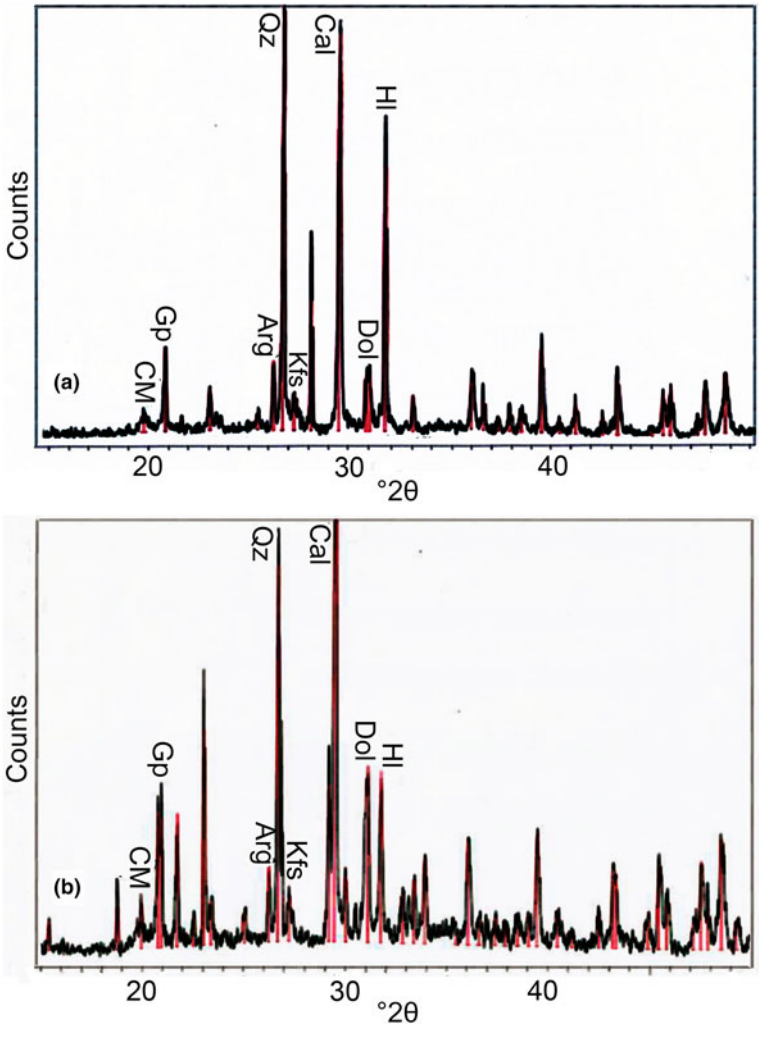

Figure 6. XRD traces of selected mudflat sediments (a) from a subsidence strip and (b) in a sinkhole. Arg = aragonite; Cal = calcite; CM = clay minerals; Dol = dolomite; Gp = gypsum; Hl = halite; Kfs = K-feldspar; Qz = quartz. The mineral abbreviations are according to Warr (2020).

Table 2. Semi-quantitative mineralogical composition (normalized to 100%) of the bulk mudflat sediments sampled from subsidence strips and in clustered sinkholes.

Mudflat sediments	Calcite (%)	Aragonite (%)	Dolomite (%)	Quartz (%)	Feldspar (%)	CM (%; kaolinite)	Gypsum (%)	Halite (%)
Major peak (*d* (nm)/°2θ)	0.3035/29.40	0.3396/26.22	0.2886/30.95	0.3343/26.64	0.3250/27.40	0.4400/19.80	0.7510/11.70	0.2800/31.70
Conversion factor[a]	1.0	1.2	1.2	1.0	4.0	4.0	0.5	0.5
In subsidence strips (S-)								
S-ES-1	40	10	5	19	6	13	2	5
S-ES-2	46	14	7	17	5	10	0	1
S-ES-3	40	13	7	21	8	9	1	1
S-EG-1	40	13	4	22	8	8	2	3
S-EG-2	37	13	7	20	7	12	1	3
S-MB-1	43	13	6	19	6	13	0	0
S-MB-2	47	12	6	17	6	9	1	2
S-MB-3	43	13	7	15	4	7	2	9
S-MB-4	43	12	6	18	6	9	2	4
S-MB-5	42	11	5	22	7	12	0	1
In clustered sinkholes (H-)								
H-ES-4	36	11	6	17	6	11	4	9
H-ES-5	38	12	5	20	8	8	4	5
H-ES-6	34	12	6	19	7	10	5	7
H-ES-7	37	11	6	17	6	9	6	8
H-EG-3	34	10	5	20	8	14	3	6
H-EG-4	39	10	5	20	6	9	4	7
H-EG-5	37	12	6	16	6	14	3	6
H-MB-7	44	11	6	17	6	9	2	5
H-MB-8	38	15	6	16	6	12	2	5
H-MB-12	37	9	5	19	7	13	4	6

[a]The conversion factors are according to Ganor *et al.* (2000).
CM = clay minerals.

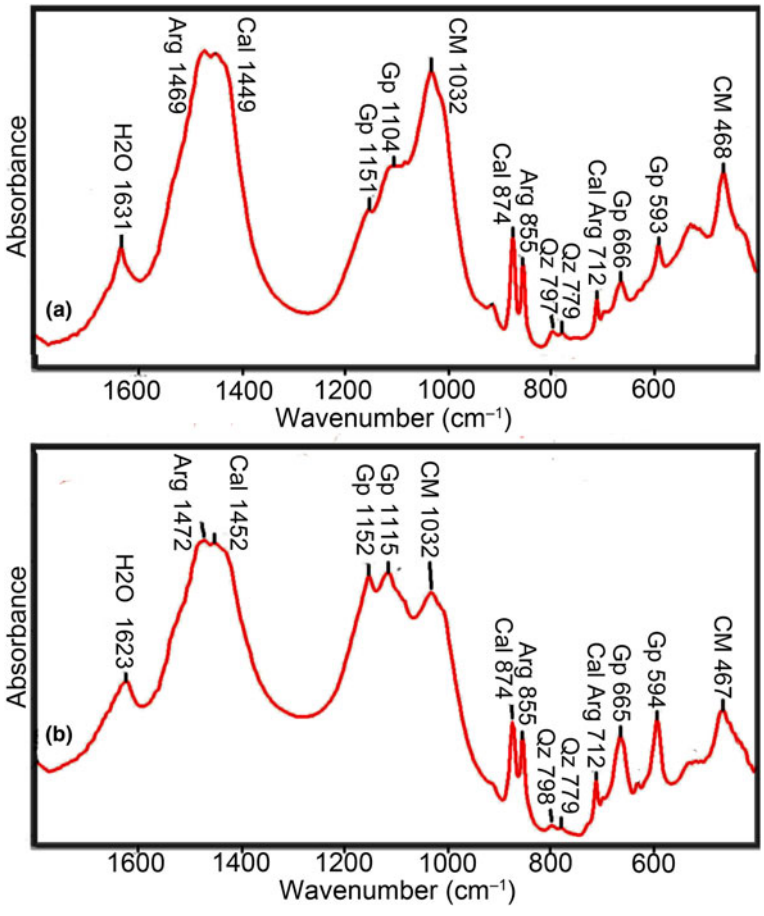

Figure 7. FTIR spectra of selected mudflat sediments (a) from subsidence strips and (b) in clustered sinkholes. Arg = aragonite; Cal = calcite; CM = clay minerals; Gp = gypsum; Qz = quartz.

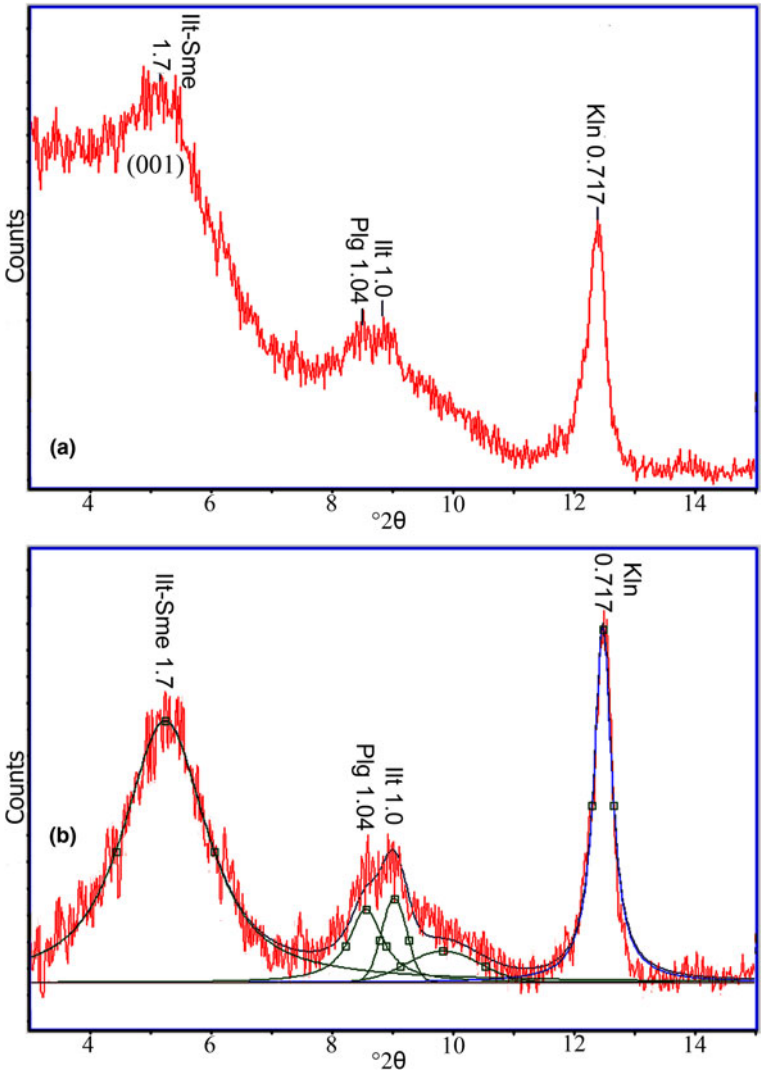

Figure 8. XRD traces of the clay mineral composition obtained from a selected mudflat sediment. (a) Original XRD trace and (b) XRD trace after baseline correction and curve-fitting. Ilt = discrete illite; Ilt-Sme: R0 mixed-layer illite–smectite; Kln = kaolinite; Plg = palygorskite.

(Fig. 8a; Eslinger & Pevear, 1988; Moore & Reynolds, 1997). The XRD traces of the heated samples indicate the presence of minor to trace amounts of chlorite (<3%).

Table 3 lists the relative abundances of the clay minerals (namely R0 mixed-layer illite–smectite, kaolinite, discrete illite and palygorskite) in the decalcified clay fractions obtained from the mudflat sediments. Clay minerals usually have broad XRD peaks; therefore, their relative amounts were calculated from the areas of the major XRD peak of each clay mineral after ethylene glycol solvation (Fig. 8b) using curve-fitting in *GRAMS/AI 32* software (Shoval & Zlatkin, 2009). Table 3 gives the *d* (nm)/°2θ values of the major XRD peak for each of the identified clay minerals.

The fraction of the illite layers in the R0 mixed-layer illite–smectite is estimated to be <15%. This is obtained by calculating the 'saddle' value of the major peak of the clay mineral in the original XRD traces (e.g. Fig. 8a; Inoue *et al.*, 1989; Sandler & Herut, 2000). The identified discrete illite (Table 3) is non-expandable without mixed layering.

FTIR spectroscopy analysis of the decalcified clay fractions

Figure 9 shows a curve-fitted FTIR spectrum in the OH-stretching region of a decalcified clay fraction obtained from a selected mudflat sediment. Curve-fitting of the FTIR spectrum enables the identification of illite–smectite in a mixture along with kaolinite (Shoval, 2004), according to their characteristic OH-stretching bands (Farmer, 1974). The sharp OH-stretching band of the kaolinite at 3620 cm^{-1} overlaps with the broad OH-stretching band of the illite–smectite, whereas the kaolinite band at 3696 cm^{-1} does not overlap with any illite–smectite band (Fig. 9). The results confirm the coexistence of illite–smectite and kaolinite in the decalcified clay fractions.

SEM images of decalcified clay fractions

Figure 10 shows a SEM (secondary electron) image of a decalcified clay fraction obtained from a selected mudflat sediment. The image shows fine-grained textures of clay platelets and grains of minerals of ~2 μm in size. The microstructure of the clay platelets observed in the SEM image is typical of a detrital clay (Fig. 10).

Major element composition of mudflat sediments

The EDS results regarding the major element composition (wt.%) of mudflat sediments sampled from subsidence strips and in clustered sinkholes are listed in Table 4. The elements identified are

Table 3. XRD results of the relative amounts (normalized to 100%) of the clay minerals in decalcified clay fractions obtained from the mudflat sediments. The *d*-values of the (001) peak of R0 mixed-layer illite–smectite in the decalcified clay fractions of the individual samples after ethylene glycol solvation have been included.

Decalcified clay fractions	R0 mixed-layer illite–smectite (*d* (nm))	R0 mixed-layer illite–smectite (%)	Kaolinite (%)	Illite (%)	Palygorskite (%)
Major peak (*d* (nm)/°2θ)	(001) peak in the glycolated state	1.70/5.20	0.72/12.33	1.00/8.83	1.04/8.49
In subsidence strips (S-)					
S-ES-1	1.700	58	21	16	5
S-ES-2	1.745	55	25	11	9
S-ES-3	1.760	63	16	15	6
S-EG-1	1.762	64	24	7	5
S-EG-2	1.820	65	24	3	8
S-MB-1	1.762	39	25	27	9
S-MB-2	1.760	60	20	15	5
S-MB-3	1.750	50	25	17	8
S-MB-4	1.748	46	28	7	19
S-MB-5	1.688	69	19	8	4
In sinkholes (H-)					
H-ES-4	1.731	69	19	8	4
H-ES-5	1.750	65	17	12	6
H-ES-6	1.708	56	29	14	1
H-ES-7	1.675	47	38	10	5
H-EG-3	1.710	65	24	3	8
H-EG-4	1.660	63	24	12	1
H-EG-5	1.738	58	23	17	2
H-MB-7	1.752	54	26	5	15
H-MB-8	1.762	57	25	6	12
H-MB-12	1.744	63	26	5	6

Na, K, Ca, Mg, Al, Si, Sr and Cl. This composition confirms the existence of precipitated salts in the mudflat sediments. Al and Si sources are mainly from clay minerals, Ca is from calcite, aragonite and dolomite, Mg is from dolomite and Mg-salts, K is from illite–smectite, K-feldspar and K-salts and Na and Cl are from halite.

Major element composition of the sinkhole brine

Table 5 lists the chemical analysis results regarding the major element composition (mg L^{-1}) of sinkhole brine, local saline water and sea water. The elements detected in the saline water are Na, K, Ca, Mg, Sr, Br and Cl. Variations in the amounts of Na and Mg in sinkhole brine (Table 5) are related to the precipitation of halite crystals from the brine (Fig. 5), which decreases the proportion of dissolved Na and thus increases the proportion of the dissolved Mg. The total dissolved salts (TDS; mg L^{-1}) of some sinkhole brines exceed that of the Dead Sea water, is higher than that of the local saline water and is much higher than that of the Mediterranean Sea water (Table 5).

Discussion

Clayey sediments in the environment of the exposed mudflats

The retreat of the Dead Sea and the lowering of the base level in recent decades exposed the littoral clay sediments on the shore, the mudflats (Fig. 3a) and the developed subsidence strips and clustered sinkholes (Fig. 4). Based on field observations and laboratory analyses, the present study characterizes the clayey

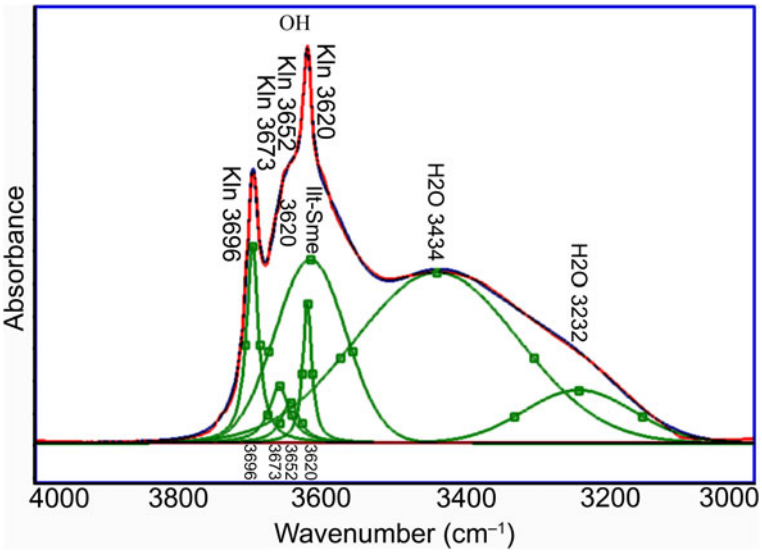

Figure 9. Curve-fitted FTIR spectrum in the OH-stretching region of a decalcified clay fraction obtained from a selected mudflat sediment. Ilt-Sme = illite–smectite; Kln = kaolinite.

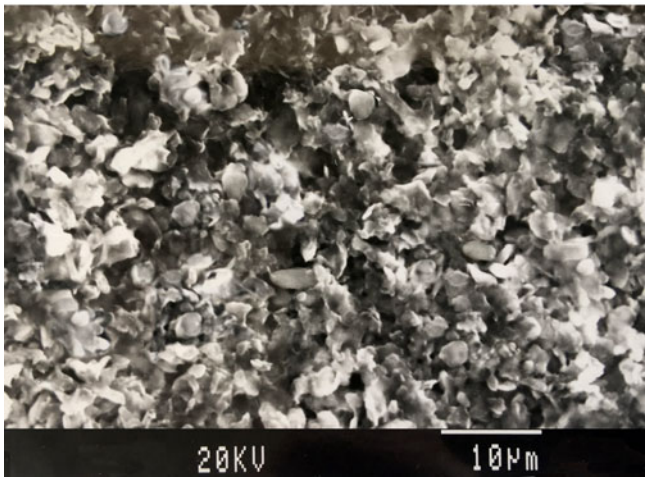

Figure 10. SEM (secondary electron) image of a decalcified clay fraction obtained from a selected mudflat sediment. The microstructure of the clay platelets is typical of a detrital clay.

sediments in the environment of the exposed mudflats on the western Dead Sea shore.

Composition of the mudflat sediments

The mineralogical composition of the bulk mudflat sediments sampled from the subsidence strips and in clustered sinkholes (Fig. 4) includes clay minerals and carbonate minerals (calcite, aragonite and dolomite) with some quartz and feldspar (Table 2), and frequently gypsum and halite (Fig. 6). The clay mineral composition of these samples is R0 mixed-layer illite–smectite and kaolinite with some discrete illite and palygorskite (Fig. 8 & Table 3). The microstructure of the clay platelets is typical of a detrital clay (Fig. 10).

Sources of detrital clays in the mudflat sediments

Source of the detrital clay minerals and fine-grained calcite and dolomite in the Late Quaternary units deposited in the Dead Sea periphery (Fig. 2) were reported by Bookman *et al.* (2004), Garber *et al.* (1987) and Lu *et al.* (2020). Haliva-Cohen *et al.* (2012) studied the sources of the fine detritus material that was transported and deposited in the Late Quaternary units in the Dead Sea periphery and reported several sources of the fine detritus materials, namely flood material, desert dust and loess from the Dead Sea watershed. The main minerals of the detritus material in the lake formations are quartz and calcite, minor dolomite, clays and feldspars. The clays are predominantly mixed-layer illite–smectite with small amounts of kaolinite and minor to trace amounts of palygorskite and chlorite.

Table 4. EDS results regarding the major element composition (wt.%) of mudflat sediments sampled from subsidence strips and in clustered sinkholes. The analytical error is ~2%.

Mudflat sediments	Na	K	Ca	Mg	Al	Si	Sr	Cl
In subsidence strips (S-)								
S-ES-2	1.1	2.3	16.7	9.6	5.0	17.0	0.2	39.5
S-ES-3	1.2	1.9	16.8	15.8	4.5	10.5	0.2	43.8
S-EG-2	2.1	1.7	21.4	12.6	5.0	12.0	0.1	40.1
S-MB-2	2.0	6.9	25.2	13.5	2.5	11.2	0.2	35.5
S-MB-5	1.0	6.0	17.5	15.2	3.2	12.4	0.2	40.9
In sinkholes (H-)								
H-ES-4	9.6	0.9	26.3	11.4	1.9	6.8	0.1	32.8
H-ES-5	8.8	1.9	10.3	19.5	0.2	2.6	0.1	54.9
H-ES-6	10.5	5.4	12.4	15.7	1.7	4.3	0.3	48.2
H-ES-7	12.0	1.2	29.6	8.1	2.9	11.8	0.3	25.0
H-EG-5	9.6	4.6	14.3	15.0	2.6	6.7	0.1	44.5
H-MB-7	7.9	1.7	29.9	9.2	5.3	15.5	1.0	21.4

An imported source for the detrital clay in the Late Quaternary sediments of the Dead Sea periphery was the material of the seasonal floods (Haliva-Cohen *et al.*, 2012; Lu *et al.*, 2020) that was transported to the Dead Sea periphery from the weathering and erosion of the rocks exposed at the margins of the Dead Sea Basin and adjacent regions (Fig. 2). The main units exposed at the margins are Upper Cretaceous carbonate rocks (Fig. 2). On the eastern side of the Dead Sea Basin, Cambrian to Lower Cretaceous clastic rocks are also exposed.

Data on the accessory clay minerals in the Upper Cretaceous carbonate rocks are available from the studies of the corresponding units in the Negev region. Illite is dominant in the Lower Palaeozoic rocks, illite and kaolinite are dominant in the Nubian Mesozoic rocks and smectite is dominant in rocks of the large marine transgression of the Upper Cretaceous (Bentor *et al.*, 1963). The clays in the Turonian sequence in the north-eastern Negev are dominated by R0 or $R \geq 1$ mixed-layer illite–smectite along with minor discrete illite and trace chlorite, quartz and goethite (Sandler & Saar, 2007). Finally, the Senonian to Eocene clays at the south-eastern Negev are dominated by smectitic illite–smectite accompanied by detrital kaolinite, discrete illite, palygorskite and occasional sepiolite (Shoval, 2004). Following these observations, a large part of the R0 mixed-layer illite–smectite in the composition of the mudflat sediments (Fig. 8 & Table 3) was derived from the transport of detritus from weathering and erosion of the Upper Cretaceous rocks exposed at the margins of the Dead Sea Basin and adjacent regions (Fig. 2).

The contribution of wind-blown materials that settle over the exposed surfaces provided an additional source for the detritus in the Late Quaternary units deposited in the Dead Sea periphery and the Negev region. The contribution of desert dust transported from North African and Arabian deserts has been documented in previous studies (Ganor *et al.*, 1991; Ganor & Foner, 2001: Israelevich *et al.*, 2003; Sandler, 2013).

The desert dust deposits over the Dead Sea region consist of smectite, kaolinite, illite and minor amounts of palygorskite with calcite, dolomite, quartz, feldspars, some apatite and soluble salts (Singer *et al.*, 2003). In addition, the most common minerals in the suspended dust over the Dead Sea region include quartz and kaolinite with feldspar, apatite and dolomite (Singer *et al.*, 2004). Thick sequences of desert loess have accumulated from desert dust settling in the northern Negev (Bruins & Yaalon, 1979). In addition, desert dust constitutes an important part of soils in these northern regions (Yaalon, 1997).

Following these observations, a large part of the kaolinite in the composition of the mudflat sediments (Fig. 8 & Table 3) was derived from desert dust that has settled in the region (Singer *et al.*, 2004).

Saline environment of the mudflat sediments

The mudflat sediments are situated in the saline environment of the Dead Sea shore, which is affected by the contact with the Dead Sea water (Table 5). Deposition of the mudflat sediments took

Table 5. Chemical analysis results regarding the major element composition (mg L^{-1}) of sinkhole brine, local saline water, Dead Sea water and Mediterranean Sea water. The TDS (mg L^{-1}) and the reproducibility error (RE %) of the analytical data are included.

Saline water	Na	K	Ca	Mg	Sr	Br	Cl	TDS	RE %
Sinkhole brine (B-)									
B-ES-1	2600	1600	39 200	93 000	700	12 000	339 000	488 100	0.3
B-MB-14	12 360	13 050	25 640	66 838	463	8600	265 620	392 571	0.4
B-MB-15	31 953	4664	14 927	24 517	252	3250	151 950	231 513	−0.6
B-MB-16	37 293	8165	17 157	45 032	304	5300	222 260	335 511	0.5
B-EG-7	92 810	2917	7114	13 686	140	2000	197 000	315 667	0.1
B-EG-8	16 780	10 350	26 134	60 400	496	8000	254 675	376 835	0.0
B-EG-9	97 395	2236	6070	11 130	115	1650	196 000	314 596	−0.3
Local saline water (W-)									
W-ES-2	3950	840	2460	4074	31	500	21 130	35 716	−0.6
W-ES-3	940	175	475	776	8	600	4180	7562	−1.0
W-EG-4	11 655	1830	4818	75	8274	49 000	1120	81 372	−0.5
Sea water									
W-DS-1	31 370	7780	18 900	48 200	342	6200	228 280	341 072	−0.3
W-MS-1	12 200	442	476	1480	–	65	22 350	40 128	

place in a lacustrine–littoral environment of the Dead Sea periphery (Yechieli *et al.*, 1993). Their exposure in recent decades is a result of the retreat of the Dead Sea (Fig. 3a).

The Dead Sea water is saturated to oversaturated with respect to aragonite, anhydrite and halite (Gavrieli *et al.*, 1989, 2002). Gypsum is the actual Ca-sulfate mineral that precipitates from

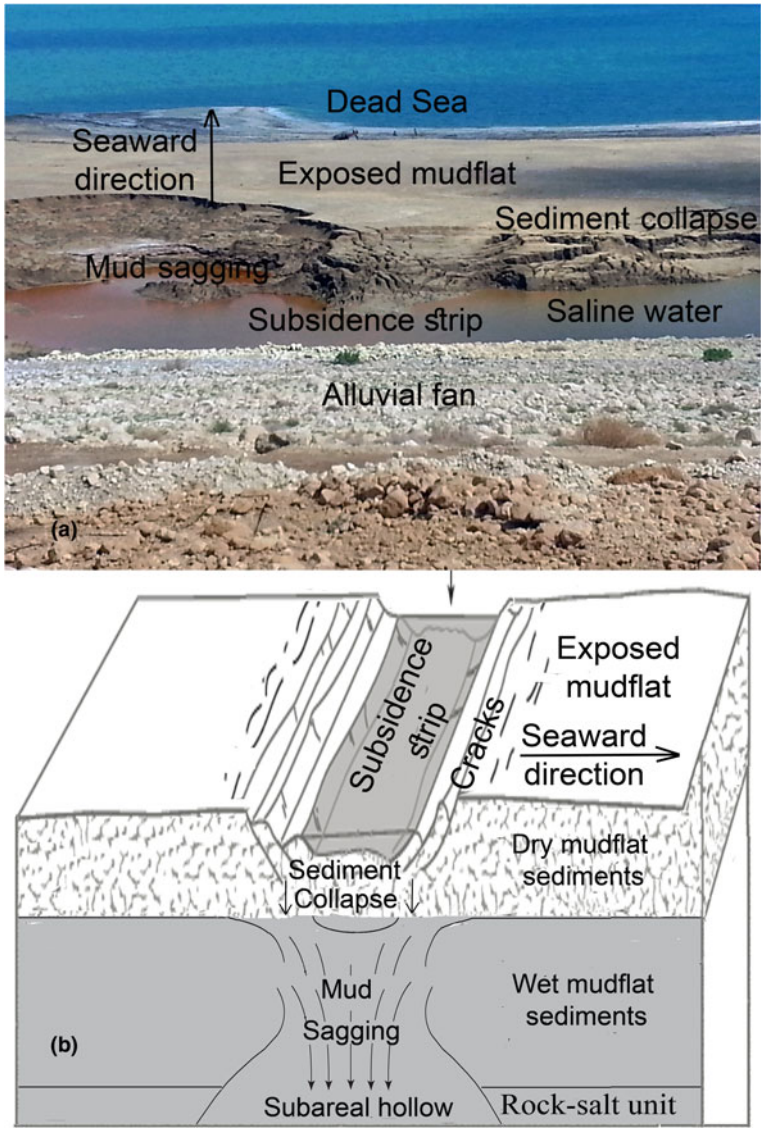

Figure 11. The formation of the subsidence strips in the exposed mudflats. (a) Subsidence of mudflat sediments forms subsidence strips and involves mud sagging of wet clayey sediments in the subsurface and sediment collapse of dry clayey sediments near the surface (at Ein-Samar coast). (b) An illustration of the subsiding processes by mud sagging and sediment collapse.

the Dead Sea water. Crystallization of aragonite (possibly with some gypsum) from the surface water formed the white aragonite laminae of the Dead Sea sediments, whereas gypsum was crystallized on exposed and submerged surfaces along the Dead Sea shores (Neev & Emery, 1967). In recent decades, halite precipitates from the Dead Sea water (Steinhorn, 1983).

The saline environment of the mudflat sediments is indicated by the accumulation of brine and precipitation of salts at the bottoms of subsidence strips and in sinkholes (Fig. 5). The TDS of some sinkhole brine exceeds that of the Dead Sea water (Table 5), which results in precipitation of salts (Fig. 5). The mineral precipitates from the sinkhole brine are halite and gypsum with some carnallite and bischofite (Zilberman-Kron, 2008).

Clays in the saline environment of the mudflat sediments

Clay diagenesis under saline environmental conditions has been reported in alkaline lakes (e.g. Singer & Stoffers, 1980) and continental evaporitic environments (Calvo *et al.*, 1995). Although the detrital R0 mixed-layer illite–smectite in the mudflat sediments is situated in the saline environment of the Dead Sea shore, no significant illitization is observed in the detrital clay. The R0 mixed-layer illite–smectite in the mudflat sediments (Table 3) is similar to that in the depositional detrital clay (Nathan *et al.*, 1990, 1992; Haliva-Cohen *et al.*, 2012). The clay platelet microstructure of the mixed-layer illite–smectite observed in the SEM image (Fig. 10) is typical of a detrital, not authigenic clay.

The presence of small amounts of palygorskite in the composition of the mudflat sediments is explained by the contribution from the detritus sources. However, the larger amounts of palygorskite occurring in several samples (Table 3) may reflect some authigenic origin of this clay in the saline environment. Palygorskite authigenesis has been reported in continental saline evaporitic environments (Calvo *et al.*, 1995). This process occurs in conditions of magnesium-enriched brine in a hot-arid climate (Jones, 1986).

The lack of significant clay diagenesis in the sub-recent sediments of the Dead Sea has been attributed to the young Holocene age of these sediments, the relatively low burial temperature and the low pH (6.1–6.7; Nathan *et al.* 1990, 1992). Diagenesis most likely occurs only after deeper burial, at temperatures >50–60°C and for a longer period under saline conditions (Nathan *et al.*, 1994).

By contrast to the detrital smectitic illite–smectite in the composition of the mudflat sediments, a gradual illitization of smectite and a greater authigenesis of palygorskite were reported in the calcareous shale units of the Pliocene Sedom Formation in the Mount Sodom salt diapir in the Dead Sea Basin (Shoval & Zlatkin, 2009). The illitization was attributed to deeper burial conditions and a longer period in contact with the rock salts of this Formation. Diagenesis of trioctahedral clays in a Miocene to Pleistocene sedimentary–magmatic sequence in the Dead Sea Rift was reported by Sandler *et al.* (2001).

Formation of the subsidence strips in the exposed mudflats

The subsidence strips with clustered sinkholes were formed in the exposed mudflats as part of the adjustment of the Dead Sea periphery to the lowering of the base level as a result of the retreat of the Dead Sea. The origin of the sinkholes on the shore of the Dead Sea is related to the subsiding of sediments following dissolution and salt karstification within a subareal rock-salt unit (Frumkin & Raz, 2001; Yechieli *et al.*, 2016; Ezersky *et al.*, 2017; Watson *et al.*, 2019; Ezersky & Frumkin, 2020, 2021; Abelson, 2021).

The field observations in the studied area reveal that the subsidence of mudflat sediments during the formation of the subsidence strips usually involves mud sagging of wet clayey sediments in the subsurface and sediment collapse of dry clayey sediments near the surface (Fig. 11a). The mud sagging of wet clayey sediments is observed within subsidence strips inundated with water, and sediment collapse of dry clayey sediments is visible on their walls (Fig. 11a). Figure 11b provides an illustration of the subsiding processes by mud sagging and sediment collapse.

The development of the subsidence strips in the Dead Sea shore may serve as a preferential subsurface pathway for groundwater that allows dissolution and salt karstification within a subareal rock-salt unit and promotes the formation of clustered sinkholes.

Contribution of the clay sediments to the subsiding

The geotechnical characteristics of sediments on the western shore of the Dead Sea were reported by Ezersky & Livne (2013) and on the eastern shore by Taqieddin *et al.* (2000), Khlaifat *et al.* (2010) and Salameh *et al.* (2019). Geotechnical studies of evaporitic, lacustrine sediments in the saline environment of the Dead Sea area were reported by Frydman *et al.* (2008, 2014). Viscoelastic modelling of sinkhole precursory subsidence was proposed by Baer *et al.* (2018).

The analyses of the mudflat sediments reflect the contribution of the clayey sediments to the origin of the subsidence strips on the exposed mudflats. During development of the subsidence strips, the mud sagging of wet clayey sediments in the subsurface (Fig. 11a) is favoured by their muddy behaviour under wet conditions due to the majority of swelling smectitic clay (Table 3) and the soaking in saline water and brine rich in sodium (Table 5). The sediment collapse of the dry clayey sediments near the surface (Fig. 11) is promoted by their fine-grained unconsolidated textures (Fig. 3b) consisting of clay and carbonate particles (Table 2), which are devoid of significant cohesion (Ezersky & Livne, 2013).

Future prospects

The extending of the clustered sinkholes along the shore of the Dead Sea is usually attributed to subsidence of the sediments along lineaments that track some of the existing tectonic faults of the Dead Sea Rift in the Dead Sea shore. The field observations reveal features of mass movement seaward in the mudflat sediments on the Dead Sea shore. As a future prospect, it is recommended that we examine whether the seaward mass movement (sediment creep) leads to tension in the mudflat sediments that breaks continuity and generates subsidence strips. Indeed, the subsidence strips extend approximately parallel to the shoreline, they gradually widen over time and they are progressively inundated with saline water. In addition, it is recommended that we examine whether the narrow coastal bays along the curved Dead Sea shoreline are scars resulting from the slumping of littoral clayey sediments on the coastal edge towards the subsea slope.

Summary and conclusions

(1) Exposed mudflats appeared in recent decades on the western shore of the Dead Sea as part of the adjustment of the Dead

Sea periphery to the retreat of the Dead Sea. Based on field observations and laboratory analyses, the present study characterizes the clayey sediments in the environment of the exposed mudflats on the western Dead Sea shore.

(2) The mudflat sediments in subsidence strips and clustered sinkholes consist of clay minerals and carbonates (calcite, aragonite and dolomite) with some quartz and feldspar and frequently gypsum and halite. The clay minerals present are R0 mixed-layer illite–smectite and kaolinite with minor discrete illite and palygorskite.

(3) A large part of R0 mixed-layer illite–smectite in the mudflat sediments was derived from the transport of detritus from weathering and erosion of the Upper Cretaceous rocks that were exposed at the margins of the Dead Sea Basin and adjacent regions. A large part of the kaolinite in the composition of the mudflat sediments was derived from desert dust that settled in the region.

(4) Although the detrital R0 mixed-layer illite–smectite in the mudflat sediments occurs in the saline environment of the Dead Sea shore, it does not show significant illitization. The R0 mixed-layer illite–smectite in the composition of the mudflat sediments is similar to that in the depositional detrital clay. The clay platelet microstructure of the R0 mixed-layer illite–smectite observed using SEM is typical of a detrital origin.

(5) The presence of small amounts of palygorskite in the composition of the mudflat sediments is explained by the contribution from the detrital sources. However, the larger amounts of palygorskite occurring in several samples may reflect some authigenic origin of this clay in the saline environment.

(6) Subsidence strips with clustered sinkholes were formed in the exposed mudflats. The subsidence of mudflat sediments in the subsidence strips usually involves mud sagging of wet clayey sediments in the subsurface and sediment collapse of dry clayey sediments near the surface.

(7) The mud sagging of wet clayey sediments in the subsurface during the development of the subsidence strips is favoured by their muddy behaviour under wet conditions due to the majority of swelling smectitic clay and the soaking in saline water and brine rich in sodium. The sediment collapse of the dry clayey sediments near the surface is promoted by their fine-grained unconsolidated textures consisting of clay and carbonate particles, which are devoid of significant cohesion.

Acknowledgements. The analyses were performed using the laboratory facilities of the Geological Survey of Israel and of the Institute of Earth Sciences, The Hebrew University of Jerusalem. Part of this study was conducted whilst the author was a visiting scientist at the Institute of Earth Sciences at The Hebrew University of Jerusalem. The author expresses his appreciation for Professor Oded Navon of this institute for his collaboration.

Financial support. This research was supported by the Open University of Israel's Research Authority (Award Number: 37226 in year 2018). This support is gratefully acknowledged.

Conflicts of interest. The contributing author has no conflicts of interest to declare. The author is the sole contributor. The work submitted is an original scientific study (research article) and was prepared and written by the author as a professor at the Open University of Israel. The contributing author consents for publication in this journal. There are no biological applications.

Data availability. The raw database is available from the contributing author. The data are mainly based on field observations and laboratory analyses by the contributing author. All field photographs are of the author and were taken by the author himself in the field.

Declaration. This manuscript has not previously been published elsewhere, either in full or in part. While under review for *Clay Minerals*, it will not be submitted to any other publication.

References

Abelson M. (2021) Hydrological and geological controls on the evolution of the Dead Sea sinkholes. Pp. 273–298 in: *The Many Facets of Israel's Hydrogeology* (U. Kafri & Y. Yechieli, editors). Cham, Switzerland: Springer.

Abelson M., Yechieli Y., Crouvi O., Baer G., Wachs D., Bein A. & Shtivelman V. (2006) Evolution of the Dead Sea sinkholes. Pp. 241–253 in: *New Frontiers in Dead Sea Paleoenvironmental Research* (Y. Enzel, A. Agnon & M. Stein, editors). Boulder, CO, USA: Geological Society of America.

Al-Halbouni D., Holohan E.P., Saberi L., Alrshdan H., Sawarieh A., Closson D. *et al.* (2017) Sinkholes, subsidence and subrosion on the eastern shore of the Dead Sea as revealed by a close-range photogrammetric survey. *Geomorphology*, **285**, 305–324.

Arkin Y. & Gilat A. (2000) Dead Sea sinkholes – an ever-developing hazard. *Environmental Geology*, **39**, 711–722.

Avni Y., Lensky N., Dente E., Shviro M., Arav R., Gavrieli I. *et al.* (2016) Self-accelerated development of salt karst during flash floods along the Dead Sea coast, Israel. *Journal of Geophysical Research: Earth Surface*, **121**, 17–38.

Baer G., Schattner U., Wachs D., Sandwell D., Wdowinski S. & Frydman S. (2002) The lowest place on Earth is subsidence – an InSAR (interferometric synthetic aperture radar) perspective. *Geological Society of America Bulletin*, **114**, 12–23.

Baer G., Magen Y., Nof R.N., Raz E., Lyakhovsky V. & Shalev E. (2018) InSAR measurements and viscoelastic modeling of sinkhole precursory subsidence: implications for sinkhole formation, early warning, and sediments properties. *Journal of Geophysical Research: Earth Surface*, **123**, 678–693.

Belmaker R., Lazar B., Stein M., Taha N. & Bookman R. (2019) Constraints on aragonite precipitation in the Dead Sea from geochemical measurements of flood plumes. *Quaternary Science Reviews*, **221**, 105876.

Bentor Y.K., Bodenheimer W. & Heller L. (1963) A reconnaissance survey of the relationship between clay mineralogy and geological environment in the Negev (southern Israel). *Journal of Sedimentary Research*, **33**, 874–903.

Bookman R., Enzel Y., Agnon A. & Stein M. (2004) Late Holocene lake level of the Dead Sea. *Geological Society of America Bulletin*, **116**, 555–571.

Bruins H.J. & Yaalon D.H. (1979) Stratigraphy of the Netivot section in the desert loess of the Negev (Israel). *Acta Geologica Academiae Scientiarum Hungaricae*, **22**, 161–169.

Calvo J.P., Blanc-Valleron M.M., Rodriguez-Arandia J.P., Rouchy J.M. & Sanz M.E. (1995) Authigenic clay minerals in continental evaporitic environments. Pp. 129–151 in: *Palaeoweathering, Palaeosurfaces and Related Continental Deposits* (M. Thiry & R. Simon-Coinçon, editors). Hoboken, NJ, USA: Wiley.

Eslinger E. & Pevear D. (1988) *Clay Minerals for Petroleum Geologists and Engineers*. Tulsa, OK, USA: Society of Economic Paleontologists and Mineralogists, 405 pp.

Ezersky M.G. & Frumkin A. (2020) Identification of sinkhole origin using surface geophysical methods, Dead Sea, Israel. *Geomorphology*, **364**, 107225.

Ezersky M.G. & Frumkin A. (2021) Subareal morphology affected by groundwater aggressiveness: sinkhole susceptibility above karstified salt, Dead Sea. *Geomorphology*, **375**, 107525.

Ezersky M.G. & Livne E. (2013) Geotechnical and geophysical properties of soils in the Dead Sea sinkhole problem. P. cp-354 in: *Near Surface Geoscience 2013 – 19th EAGE European Meeting of Environmental and Engineering Geophysics*. Utrecht, The Netherlands: European Association of Geoscientists and Engineers.

Ezersky M.G., Legchenko A., Eppelbaum L. & Al-Zoubi A. (2017) Overview of the geophysical studies in the Dead Sea coastal area related to evaporite karst and recent sinkhole development. *International Journal of Speleology*, **46**, 277–302.

Farmer V.C. (1974) The layer silicates. Pp. 331–363 in: *The Infrared Spectra of Minerals* (V.C. Farmer, editor). London, UK: Mineralogical Society.

Frumkin A. & Raz E. (2001) Collapse and subsidence associated with salt karstification along the Dead Sea. *Carbonates and Evaporites*, **16**, 117–130.

Frydman S., Charrach J. & Goretsky I. (2008) Geotechnical properties of evaporite soils of the Dead Sea area. *Engineering Geology*, **101**, 236–244.

Frydman S., Charrach J. & Goretsky I. (2014) A geotechnical study of evaporitic, lacustrine sediments in the saline environment of the Dead Sea area. *Engineering Geology*, **181**, 309–322.

Ganor E. & Foner H.A. (2001) Mineral dust concentrations, deposition fluxes and deposition velocities in dust episodes over Israel. *Journal of Geophysical Research: Atmospheres*, **106**, 18431–18437.

Ganor E., Foner H.A., Brenner S., Neeman E. & Lavi N. (1991) The chemical composition of aerosols settling in Israel following dust storms. *Atmospheric Environment. Part A. General Topics*, **25**, 2665–2670.

Ganor E., Deutsch Y. & Foner H.A. (2000) Mineralogical composition and sources of airborne settling particles on Lake Kinneret (the Sea of Galilee), Israel. *Water, Air, and Soil Pollution*, **118**, 245–262.

Garber R.A., Levy Y. & Friedman G.M. (1987) The sedimentology of the Dead Sea. *Carbonates and Evaporites*, **2**, 43–57.

Garfunkel Z. (1997) The history and formation of the Dead Sea Basin. Pp. 36–55 in: *The Dead Sea: The Lake and Its Setting* (T.M. Niemi, Z. Ben-Avraham & J. Gat, editors). Oxford, UK: Oxford University Press.

Garfunkel Z. & Ben-Avraham Z. (1996) The structure of the Dead Sea Basin. *Tectonophysics*, **266**, 155–176.

Gavrieli I., Starinsky A. & Bein A. (1989) The solubility of halite as a function of temperature in the highly saline Dead Sea brine system. *Limnology and Oceanography*, **34**, 1224–1234.

Gavrieli I., Lensky N., Gazit-Yaari N. & Aharon O. (2002) *The Impact of the Proposed 'Peace Conduit' on the Dead Sea. Evaluation of Current Knowledge on Dead Sea–Seawater Mixing*. Report GSI/23/2002. Jerusalem, Israel: Geological Survey of Israel, 42 pp.

Ghazleh S.A., Abed A.M. & Kempe S. (2011) The dramatic drop of the Dead Sea: background, rates, impacts and solutions. Pp. 77–105 in: *Macro-engineering Seawater in Unique Environments: Arid Lowlands and Water Bodies Rehabilitation* (V. Badescu & R.B. Cathcart, editors). Berlin, Germany: Springer.

Haliva-Cohen A., Stein M., Goldstein S.L., Sandler A. & Starinsky A. (2012) Sources and transport routes of fine detritus material to the Late Quaternary Dead Sea Basin. *Quaternary Science Reviews*, **50**, 55–70.

Inoue A., Bouchet A., Velde B. & Meunier A. (1989) Convenient technique for estimating smectite layer percentage in randomly interstratified illite/smectite minerals. *Clays and Clay Minerals*, **37**, 227–234.

Israelevich P.L., Ganor E., Levin Z. & Joseph J.H. (2003) Annual variations of physical properties of desert dust over Israel. *Journal of Geophysical Research: Atmospheres*, **108**, 10.1029/2002JD003163.

Jones B.F. (1986) Clay mineral diagenesis in lacustrine sediments. *US Geological Survey Bulletin*, **1578**, 291–300.

Khlaifat A., Al-Khashman O. & Qutob H. (2010) Physical and chemical characterization of Dead Sea mud. *Materials Characterization*, **61**, 564–568.

Leontopoulou G., Christidis G.E., Rousakis G., Müller N.S., Papatheodorou G. & Geraga M. (2021) Provenance analysis of sediments in the south-east Aegean during the Upper Quaternary: a composite approach based on bulk and clay mineralogy and geochemistry. *Clay Minerals*, **56**, 229–249.

Lipchin C.D., Antonius R., Rishmawi K., Afanah A., Orthofer R. & Trottier J. (2004) *Public perceptions and attitudes towards the declining water-level of the Dead Sea Basin: a multi-cultural analysis*. Palestinian and Israeli Environmental Narratives, York University, Toronto, Canada. Retrieved from http://proxy.arij.org/deadseaproject/Publications/Lipchinpaper.pdf

Lu Y., Bookman R., Waldmann N. & Marco S. (2020) A 45 kyr laminae record from the Dead Sea: implications for basin erosion and floods recurrence. *Quaternary Science Reviews*, **229**, 106143.

Moore D.M. & Reynolds R.C (1997) *X-Ray Diffraction and the Identification and Analysis of Clay Minerals* (2nd edition). Oxford, UK: Oxford University Press, 378 pp.

Nathan Y., Shoval S. & Sandler A. (1990) *Clays of the Dead Sea*. Report GSI/25/90. Jerusalem, Israel: Geological Survey of Israel, 12 pp.

Nathan Y., Shoval S. & Sandler A. (1992) *Dead Sea Clays*. Report GSI/21/92. Jerusalem, Israel: Geological Survey of Israel, 26 pp. (in Hebrew).

Nathan Y., Sandler A. & Shoval S. (1994) Clays of the Dead Sea. *Current Research, Geological Survey of Israel* (*GSI*), **9**, 20–23.

Neev D. & Emery K.O. (1967) The Dead Sea: depositional processes and environments of evaporites. *Geological Survey of Israel Bulletin*, **41**, 1–147.

Neev D. & Hall J.K. (1979) Geophysical investigations in the Dead Sea. *Sedimentary Geology*, **23**, 209–238.

Rogoziński R. & Maciejewska, A. (2021) Geochemistry and mineralogy of ice-dammed lake sediments of the Lębork Deposit. *Clays and Clay Minerals*, **69**, 315–327.

Salameh E., Alraggad M. & Amaireh M. (2019) Degradation processes along the new northeastern shores of the Dead Sea. *Environmental Earth Sciences*, **78**, 1–12.

Sandler A. (2013) Clay distribution over the landscape of Israel: From the hyper-arid to the Mediterranean climate regimes. *Catena*, **110**, 119–132.

Sandler A. & Herut B. (2000) Composition of clays along the continental shelf off Israel: contribution of the Nile *versus* local sources. *Marine Geology*, **167**, 339–354.

Sandler A. & Saar H. (2007) R≥1-type illite–smectite formation at near-surface temperatures. *Clay Minerals*, **42**, 245–253.

Sandler A., Nathan Y., Eshet Y., & Raab M. (2001) Diagenesis of trioctahedral clays in a Miocene to Pleistocene sedimentary–magmatic sequence in the Dead Sea Rift, Israel. *Clay Minerals*, **36**, 29–47.

Shoval S. (2004) Clay sedimentation along the southeastern Neo-Tethys margin during the oceanic convergence stage. *Applied Clay Science*, **24**, 287–298.

Shoval S. (2017) Fourier Transform infrared spectroscopy (FT-IR) in archaeological ceramic analysis. Pp. 509–530 in: *The Oxford Handbook of Archaeological Ceramic Analysis* (A. Hunt, editor). Oxford, UK: Oxford University Press.

Shoval S. & Zlatkin O. (2009) Climatic changes during the Pliocene as observed from climate-sensitive rocks and clay minerals of the Sedom Formation, the Dead Sea Basin. *Clay Minerals*, **44**, 465–482.

Shoval S., Yariv S., Michaelian K.H., Lapides I., Boudeuille M. & Panczer G. (1999) A fifth OH-stretching band in IR spectra of kaolinites. *Journal of Colloid and Interface Science*, **212**, 523–529.

Shviro M., Haviv I. & Baer G. (2017) High-resolution InSAR constraints on flood-related subsidence and evaporate dissolution along the Dead Sea shores: interplay between hydrology and rheology. *Geomorphology*, **293**, 53–68.

Singer A. & Stoffers P. (1980). Clay mineral diagenesis in two East African lake sediments. *Clay Minerals*, **15**, 291–307.

Singer A., Ganor E., Dultz S. & Fischer W. (2003) Dust deposition over the Dead Sea. *Journal of Arid Environments*, **53**, 41–59.

Singer A., Dultz S., & Argaman E. (2004) Properties of the non-soluble fractions of suspended dust over the Dead Sea. *Atmospheric Environment*, **38**, 1745–1753.

Stein M. (2001) The sedimentary and geochemical record of Neogene–Quaternary water bodies in the Dead Sea Basin – inferences for the regional paleoclimatic history. *Journal of Paleolimnology*, **26**, 271–282.

Stein M. (2014) The evolution of Neogene–Quaternary water-bodies in the Dead Sea Rift valley. Pp. 279–316 in: *Dead Sea Transform Fault System: Reviews* (Z. Garfunkel, Z. Ben-Avraham & E. Kagan, editors). Dordrecht, The Netherlands: Springer.

Steinhorn I. (1983) *In situ* salt precipitation at the Dead Sea: *Limnology and Oceanography*, **28**, 580–583.

Taqieddin S.A., Abderahman N.S. & Atallah M. (2000) Sinkhole hazards along the eastern Dead Sea shoreline area, Jordan: a geological and geotechnical consideration. *Environmental Geology*, **39**, 1237–1253.

Trindade M.J., Rocha F., Dias M.I. & Prudêncio M.I. (2013) Mineralogy and grain-size distribution of clay-rich rock units of the Algarve Basin (south Portugal). *Clay Minerals*, **48**, 59–83.

Trindade M.J., Dias M.I., Rocha F., Prudêncio M.I. & Marques R. (2018) Geochemistry of mudrock units from the Meso-Cenozoic Algarve Basin, Portugal. *Geosciences Journal*, **22**, 733–749.

Vey S., Al-Halbouni D., Haghighi M.H., Alshawaf F., Vüllers J., Güntner A. *et al.* (2021) Delayed subsidence of the Dead Sea shore due to hydrometeorological changes. *Scientific Reports*, **11**, 1–10.

Warr L.N. (2020) Recommended abbreviations for the names of clay minerals and associated phases. *Clay Minerals*, **55**, 261–264.

Watson R.A., Holohan E.P., Al-Halbouni D., Saberi L., Sawarieh A., Closson D. *et al.* (2019) Sinkholes and uvalas in evaporite karst: spatio-temporal development with links to base level fall on the eastern shore of the Dead Sea. *Solid Earth*, **10**, 1451–1468.

Yaalon D.H. (1997) Soils in the Mediterranean region: what makes them different? *Catena*, **28**, 157–169.

Yechieli Y., Magariz M., Levy Y., Weber U., Kafri U., Woelfli W. & Bonani G. (1993) Late Quaternary geological history of the Dead Sea area, Israel. *Quaternary Research*, **39**, 59–67.

Yechieli Y., Abelson M., Wachs D., Shtivelman V., Crouvi O. & Baer G. (2003) Formation of sinkholes along the shore of the Dead Sea – preliminary investigation. Pp. 184–194 in: *Sinkholes and the Engineering and Environmental Impacts of Karst* (L.B. Yuhr, E.C. Alexander Jr & B.F. Beck, editors). Reston, VA, USA: American Society Civil Engineers.

Yechieli Y., Abelson M., Bein A., Crouvi O. & Shtivelman V. (2006) Sinkhole 'swarms' along the Dead Sea coast: reflection of disturbance of lake and adjacent groundwater systems. *Geological Society of America Bulletin*, **118**, 1075–1087.

Yechieli Y., Abelson M. & Baer G. (2016) Sinkhole formation and subsidence along the Dead Sea coast, Israel. *Hydrogeology Journal*, **24**, 601–612.

Zilberman-Kron T. (2008). *The Origin and Geochemical Evolution of Brines in the Sinkholes along the Dead Sea Coast*. Report GSI/21/08. Jerusalem, Israel: Geological Survey of Israel, 97 pp. (in Hebrew).